Influence of Polyethylene Glycol Passivation on the Surface Plasmon Resonance Induced Photothermal Properties of Gold Nanorods

Ramesh Marasini[1, 2], Arunkumar Pitchaimani[2], Tuyen Duong Thanh Nguyen[1, 2], Jeffrey Comer,[2] Santosh Aryal[1, 2] *

[1]Department of Chemistry, Kansas State University, Manhattan, KS 66506

[2]Department of Anatomy and Physiology, Nanotechnology Innovation Center of Kansas State (NICKS), , Kansas State University, Manhattan, KS 66506

*Corresponding Author: saryal@ksu.edu

Department of Chemistry, Kansas State University, Manhattan, KS and

Nanotechnology Innovation Center of Kansas State (NICKS), Department of Anatomy and Physiology, Kansas State University,

1800 Denison Avenue,

Mosier Hall P218,

Manhattan, KS 66506

Phone: 785-532-6326

Fax: 785-532-4953

ABSTRACT

Gold nanorods (AuNRs) possess unique photothermal properties due to their strong plasmonic absorption in the near-infrared region of the electromagnetic spectrum. They have been explored widely as an alternative or complement to chemotherapy in cancer treatment. However, stability of AuNRs in biological fluids is a required for their effectiveness as an injectable medicine. Coatings AuNRs in polymer polyethylene glycol (PEG) can prevent nanoparticle aggregation, enhance biocompatibility, and allow controlled release of drugs. However, these coatings can affect heat conduction and alter their photothermal behavior. Herein, we studied how functionalization of AuNRs with PEG chains of different molecular weights determined the temperature distribution of suspensions under near-infrared irradiation, cell uptake *in vitro*, and hyperthermia induced cytotoxicity. Thermogravimetric analysis of the PEG conjugated AuNRs exhibited slightly different PEG mass fractions of 12%, 12.7%, and 18.5% for PEG chains with molecular weights of 2, 5 and 10 kDa, implying distinct structures for the PEG brushes. When exposed to near infrared radiation, we found greater temperatures and temperature gradients for longer PEG chains and the lowest temperatures for unmodified (raw) AuNRs. The effect of the PEG coating on heat transport was investigated using molecular dynamics simulations, which revealed the atomic scale structure of the PEG brushed and demonstrated lower thermal conductivity for PEG-coated AuNRs than for unmodified AuNRs. We also characterized the uptake of the AuNRs into mouse melanoma cells *in vitro* and determined their ability to kill these cells when subjected to near infrared radiation. For all PEG-coated AuNRs, exposure to 10 s of near infrared radiation significantly reduced cell viability relative to unirradiated controls, with this viability further decreasing with increasing AuNR doses, indicating potential phototherapeutic effects. The 5 kDa PEG coating appeared yield the best performance, yielding significant phototoxicity at even the lowest dose considered (0.5 μg/mL), while also exhibiting colloidal high stability.

The unique photothermal properties of gold nanorods (AuNRs), due to their strong plasmonic effect at near-infrared (NIR) region, have been explored widely as an alternative to chemotherapy or in combination for cancer treatment. However, its use as an injectable medicine is greatly influenced by its stability in biological media. Therefore, studies were focused on improving the stability of AuNRs by introducing biocompatible surface functionalizations such as polyethylene glycol (PEG) coatings. Also, PEG coatings have established important trends on PEG size, shape, density, loading level, molecular weight, and charge with the ultimate goal to prevent nanoparticle aggregation, enhance biocompatibility, and sustained release of payload. However,reports have shown that surface coatings are also found to hinder the diffusion of water and thermal conductivity in the vicinity of nanoparticle surface thereby affecting the physicochemical properties. Herein, we investigated how the various PEG functionalization alters the photothermal efficacy of AuNR. For this study, NIR-responsive AuNRs were synthesized using seed-mediated growth and surface functionalized with different molecular weighted PEGs (2, 5, and 10 kDa). *In vitro,* photothermal studies of AuNRs suspension in PBS were conducted using near-infrared diode laser (λ=808 nm), which showed higher thermal stability when the surface is passivated with PEG as compared to raw AuNR. Under NIR treatment for 120 seconds, the temperature of the bulk suspension reached to 69.2 ± 2.68 °C. It has been observed that the increase and distribution of temperature throughout the suspension

were affected by PEG length. Our observation showed the following trend of temperature distribution throughout the suspension, i.e., 2kDa>5kDa>10kDa, which is presumably due to the different PEG density that hinders the diffusion of heat between AuNR surface and surrounding water thereby jacketing the heat transfer. In the case of 10 kDa PEG, the heat is greatly localized at the point of NIR laser contact suggesting that increasing PEG corona thickness retards the heat distribution. This phenomenon was further confirmed by molecular simulation, where the heat conduction through PEG brushes was mapped. Thermal conductivity was found to decrease from 1.03±0.02 [W/(K.m)] for Raw AuNR to 0.86±0.02 [W/(K.m)] for AuNR-PEG-5. Furthermore, PEG-coated AuNRs were found biocompatible and internalized into the cells with its structural integrity as depicted from hyperspectral imaging and inductively coupled plasma-mass spectroscopy. In-V*itro* viability of AuNRs internalized B16-F10 cells after irradiation with NIR laser for 10 sec shows a significant cell death with 5kDa PEG-coated AuNR. Therefore, this detailed fundamental study suggested an optimum polymer length of 5kDa of PEG is required for better passivation, colloidal stability, and photothermal effect of AuNR, which could help in rationale design consideration of AuNR for NIR induced photothermal therapy.

Keywords

Gold nanorods; polyethylene glycol; photothermal therapy; near infrared (NIR), cancer

INTRODUCTION

Gold nanorods (AuNRs) have the potential to become a powerful tool in bio-imaging, cancer targeting, and cancer therapy, owing to the ease with which their surface chemistry can be modified and their ability to strongly adsorb radiation in various regions of the electromagnetic spectrum.[1–7] The absorption of near infrared radiation (NIR) by AuNRs transforms light energy into thermal energy, which has been extensively exploited in the hyperthermia-based therapy, so-called photothermal therapy.[8,9] In the NIR region, specifically at λ=808 nm, light penetration is optimal due to minimal absorption from tissue chromophores and water. Therefore, surface plasmon resonance (SPR) induced heating is key to clinical therapy applications of AuNR involving superficial tumors, as well as those located deep within bodily tissue (using optical fibers).[10,11]

The large optical cross-sections of AuNR with tunable longitudinal surface plasmon resonance (LSPR) in the NIR makes them outstanding agents for photothermal therapy.[6,9,12,13] Given the large surface-area-to-volume ratio of AuNRs and the high strong affinity of sulfur for gold surfaces, AuNRs can be conjugated with biomolecules like proteins, DNA, siRNA, and small-molecule drugs.[14–17] Therefore, AuNRs can be engineered to deliver therapeutics and to absorb NIR radiation for ablation of tumor cells, also known as cellular hyperthermia.[18] Selectivity is achieved by directional control or by using fiber optic positioning of the incoming radiation. For a tumor that is deeply situated inside the body, local cellular hyperthermia is achieved by the administration of AuNR and the local application of a pulsed or continuous wave laser source.[19–24] NIR laser pulses absorbed by AuNR excite free electrons in the plasmon band, creating a pulse of hot electrons. The hot electron pulse cools rapidly through electron−phonon interactions by colliding with the gold lattice, heating it to thousands of degrees (depending on laser power) within ∼1 ps.[25] Heat is then transferred from the nanorod to its surroundings through phonon−phonon interactions on a time scale of ∼100 ps, resulting in an increase in temperature of the surrounding medium by tens of degrees.[26–28] The enhanced temperature in turn causes cell death. This treatment modality, also known as plasmonic photothermal therapy, provides an attractive method for the treatment of solid tumors in a minimally invasive manner.[24, 25] El-Sayed et al. studied the feasibility of in vivo NIR photothermal therapy using AuNRs in mice bearing subcutaneous squamous cell carcinoma xenografts.[29] AuNRs were conjugated to thiol-terminated polyethylene glycol (PEG) having a molecular mass of 5 kDa to increase biocompatibility, suppress immunogenic responses, and to decrease adsorption to the negatively charged luminal surface of blood vessels. A >96% decrease in average tumor growth was

observed within 13 days.[30–33] Similarly, using AuNRs functionalized with Arg–Gly–Asp peptides (RGD), studies have demonstrated the inhibition of cancer cell migration by targeting integrins.[34]

Although the plasmonic properties of AuNRs have been highly exploited in biomedical research and applications, major concerns for achieving optimum photothermal effects are the colloidal stability of AuNRs in biological media and the blocking of heat transport from the surface of AuNRs to the surrounding medium by thick coatings. Therefore, suitable surface functionalization is necessary for stable, biocompatible and long-circulating nanoparticles.[35–38] Preferably, the surface passivating material should first have a strong affinity for the nanoparticle surface and also provide them with tunable chemical functionality, good colloidal stability, and biocompatibility.[36] PEG is common material for passivation of gold nanoparticles in physiological environments, yielding high colloidal stability, biocompatibility, long blood circulation time, and preferential accumulation in tumors.[29,33,39,40] However, heat transfer from AuNRs induced by NIR radiation is greatly affected by the physical properties of the surface-conjugated material. In paritcular, PEG passivation heavily influences thermal conductivity at the gold–solvent interface, thereby altering photothermal effects at the macroscopic and microscopic levels.[41,42] A recent report from C. J. Murphy and coworkers demonstrated a decrease in the thermal conductivity of AuNR coated with the quaternary ammonium surfactant cetyltrimethylammonium bromide (CTAB), when the concentration of surfactant is above the critical micelle concentration.[43] The authors further extended their study by coating the AuNR surface layer-by-layer with polyelectrolytes and found an increase in thermal conductivity and heat capacity. It is clear that an optimizing the physical properties of the surface-conjugated ligand is important for the therapeutic outcomes. Herein, we investigated the jacketing effect of the PEG coating on photothermal cell ablation by varying the chain length of PEG conjugated to

the surface of AuNR. AuNRs passivated with PEG of different molecular masses (2, 5, and 10 kDa) were studied in detail under NIR irradiation using a diode laser (λ= 808 nm). Considering the higher NIR exposure for the surface cells versus that for deep tissue, we used a B16-F10 mouse melanoma cell line as an *in vitro* model to evaluate the therapeutic effectiveness of AuNRs.

METHODS

Chemicals and Cell Lines. Gold (III) chloride trihydrate ($HAuCl_4.3H_2O$, 99.99%), cetyl tri-methyl ammonium bromide (CTAB, 99%), sodium borohydride (98%), L-ascorbic acid (99%), silver nitrate (99%), tris-hydrochloride (tris-HCl, 99%), and 3-(4, 5- methyl thiazol-2-yl)-2, 5-diphenyltetrazolium bromide (MTT) were purchased from Sigma-Aldrich (Milwaukee, WI, USA). Polyethylene glycol carboxylic thiols (HOOC-PEG-SH) with average molecular masses of 2, 5, and 10 kilodaltons (kDa) were purchased from creative PEGWorks (North Carolina, USA). All other chemicals and reagents were of analytical grade and used as received from Fischer Scientific, USA. The mouse melanoma cell line B16–F10 was procured from ATCC and maintained in Dulbecco's modified Eagle's medium (DMEM) supplemented with 10% (v/v) fetal bovine serum (FBS) and penicillin/streptomycin (100 µg/mL) at 37 ºC in a 5% CO_2 environment.

Synthesis of Gold Nanorods (AuNRs). Near Infrared Region (NIR) responsive AuNRs were synthesized using the seed-mediated growth method as described in earlier reports.[13, 32] In brief, the seed solution was prepared by adding 250 µL of $HAuCl_4$ (0.01 M) into 10 mL of CTAB (0.1 M) under stirring. To this solution, 600 µL of freshly prepared ice cooled $NaBH_4$ (0.01 M) was quickly injected and stirred for two minutes. For the growth solution, 2 mL of $HAuCl_4$ (0.01 M) and 0.4 mL of $AgNO_3$ (0.01 M) were added to 40 mL of CTAB (0.1 M) solution. The pH of the solution was adjusted into the range of 1.0–2.0 using HCl (1.0 M) and subsequently, 0.32 mL of

ascorbic acid (0.1 M) was added to the solution under gentle mixing until the solution turned colorless. To form the AuNRs, 0.096 mL of the aged seed solution (2.5 hrs) was added to the growth solution under gentle mixing and incubated overnight at 26 ºC. The as-prepared AuNR (raw) solution capped with CTAB was stored at 4 ºC for further use.

Surface Functionalization of AuNRs. Before surface modification, the excess CTAB present in the AuNRs was removed by repeated centrifugation at 12,000 rpm for 10 mins. The AuNR pellet was re-dispersed in Mili-Q water and washed two times using the same conditions. After purification, the washed raw AuNR pellets was re-dispersed in 1 mL of Tris-HCl (50 mM) (hereafter termed "Raw AuNRs") and subsequently subjected to surface modification with the thiolated PEG (PEG-SH) of different molecular masses. For the process, 1 mL of PEG-SH (2, 5, or 10 kDa) with a concentration of 1 mg/mL dispersed in the 50 mM Tris-HCl buffer (pH = 5) were used to functionalize the surface of purified AuNR (50 mg/mL in PBS) by rotating for 1 hour at room temperature. The resulting AuNRs are hereafter referred as "AuNR-PEG-2," "AuNR-PEG-5," and "AuNR-PEG-10." The number 2, 5, and 10 in the nomenclature of each sample represents the corresponding molecular mass of the surface-conjugated PEG chains in kDa. The excess of unreacted PEG was removed by centrifugation at 12000 rpm for 10 minutes, and the pellet was re-dispersed in PBS (1x) to make a final volume of 1 mL.

Characterization of Functionalized AuNR. The surface plasmon resonance spectra of the as-prepared and surface modified AuNRs were analyzed using a UV-Vis spectrophotometer (BIOMATE-3S, Thermo Scientific) with 1.0 mm path length quartz cuvettes. The size and surface morphology were analyzed using a transmission electron microscope (FEI Technai G2 spirit Bio TWIN). The concentration of gold in all formulations were determined using inductively coupled plasma-mass spectroscopy (ICP-MS, Perkin Elmer, NEXion 350X)

following standard protocol.[37,44] The hydrodynamic size, surface charge, and zeta potential analysis of the different AuNR formulations were carried out using dynamic light scattering (DLS, Zetasizer Nano ZSP, Malvern, Worcestershire, UK). Fourier transform infrared spectroscopic (FT-IR) analysis was performed to analyze surface chemistry of AuNRs using a Nicolet™ iS™ 50 FT-IR Spectrometer (Thermo Fisher).

NIR Photothermal Efficiency. The Photothermal effects of Raw AuNR and PEGylated AuNRs suspensions were determined in a cell-free environment. Briefly, a fixed concentration of Raw AuNR, AuNR-PEG-2, AuNR-PEG-5, and AuNR-PEG-10 (20 μg/mL) were irradiated using a continuous-wave NIR diode laser with a vacuum wavelength of 808 nm (0.6 mm spot focus size, power of 21.1W/cm^2) for 0, 30, 60, 90, and 120 s. The distance of the laser spot and AuNR suspension was maintained 1 cm for all samples. During the irradiation, the temperature of AuNR suspensions in PBS (1x) was monitored by capturing images every 10 seconds using forward-looking Infrared (FLIR) thermal imaging system. For quantitative analysis, ThermaCAM™ Researcher Professional 2.8 SR1 software (FLIR system) was used to record temperature at three different locations of suspension (top, middle, and bottom) during NIR irradiation as demonstrated in Scheme 1.

Molecular Dynamics Simulations. The molecular models for performing the thermal conductivity calculations were constructed and equilibrated as described in the Supporting Information. Briefly, we created three simulation systems mimicking the Raw AuNR, AuNR-PEG-2, AuNR-PEG-5 materials used the experiments. The numbers of PEG chains per unit area of gold surface were estimated from the geometry of the AuNRs and the mass fraction of PEG determined by electron microscopy and thermogravimetric analysis, respectively. Atomistic simulations of the AuNR-PEG-10 systems were deemed infeasible due to the size of the

simulation system required for properly simulating PEG chains of that length. As illustrated in Figure 4A, each system contained a gold slab (simulated using the model of Wright et al. [SI ref. 1]), water, and (except for the Raw system) thiol-terminated PEG chains [Lee, H., Venable, R. M., MacKerell Jr, A. D., & Pastor, R. W. (2008). Molecular dynamics studies of polyethylene oxide and polyethylene glycol: hydrodynamic radius and shape anisotropy. Biophysical journal, 95(4), 1590-1599.] of the appropriate molecular masses (2 or 5 kDa). We did not attempt to model CTAB in the simulation systems, since the thermogravimetric analysis showed that the mass fraction of CTAB on the Raw AuNR surfaces was relatively small (see Figure 1E). All simulation systems had approximately the same size ($5.1\times5.3\times17.8$ nm^3) after equilibration at 300 K and atmospheric pressure. The thiolated PEG chains were relaxed in 100 ns of simulation using the program NAMD [SI ref. 4] with the thiol groups in their reduced form, allowing the brush to self-assemble into realistic arrangement before the sulfur atoms were fixed to represent covalent attachment. Subsequently, the calculations of thermal conductivity were performed using the molecular simulation program LAMMPS.[45] The thermal conductivity through the system was calculated by the algorithm of Müller-Plathe.[46] A constant heat current (2.1–2.4 μW) was imposed between the center of the system (where the gold slab was located) and the extreme ends of the system by exchange of kinetic energies every 100 simulation steps. The resulting temperature distribution (considering 20 segments of the system along the *z* axis) was measured after the system reached a steady state. Due to limitations of the Müller-Plathe algorithm's implementation in LAMMPS, covalent bonds to hydrogen and water molecules were made flexible during these simulations, requiring a 1 fs time step. The force field parameters used with NAMD were converted to LAMMPS format using a custom script (included in the SI). The simulations were run at constant volume with the overall temperature maintained at 300 K by a

Nosé-Hoover thermostat, which was previously shown not to affect the thermal conductivity calculations.[46] Each of the simulations was run more than 4 ns, with the convergence of the temperature distribution apparent after 0.5 ns. The thermal conductivity was calculated from the portion of the simulations for t>1 ns by $\lambda=QL_z/(4A\ \Delta T\ \Delta t)$, where Q is the total thermal energy transferred by the algorithm during the relevant simulation time Δt, L_z is the z dimension of the simulation system (L_z/2 is the distance between the centers of the hot and cold segments), A is the cross-sectional area of the system in the xy plane, and ΔT is the average temperature difference between the hot and cold segments in the steady state.

Cellular Uptake Study. The cellular uptake and interaction of Raw AuNR, AuNR-PEG-2, AuNR-PEG-5, and AuNR-PEG-10 were studied with B16-F10 mouse melanoma cell line. ICP-MS and dark field hyperspectral microscopy (Cytoviva Inc.) were used for quantitative and qualitative interaction studies. In short, 10 x 10^3 B16-F10 cells were seeded in an 8- chambered glass slide and incubated for 24hr. Monolayer adhered cells treated with the equivalent concentration of Raw AuNR, AuNR-PEG-2, AuNR-PEG-5, and AuNR-PEG-10 (5 µg/mL) and incubated over the period (6 and 24 hr). After incubation, an excess of AuNR was removed, and cells were washed with PBS and fixed with 4% paraformaldehyde. The cellular uptake was accessed by directly observing cells under a dark-field hyperspectral microscope, and the corresponding hyperspectral spectra of the Raw AuNR, AuNR-PEG-2, AuNR-PEG-5, and AuNR-PEG-10 were recorded, respectively.

Quantification of Gold by ICP-MS. The concentration of gold (Au) in the cell was quantified by using ICP-MS following standard protocol.[37,44] Briefly, cells containing internalized AuNR were detached, washed and collected as a palette. Cell palette were digested with 1000 µL of 37% HCl and 300 µL of 70% HNO_3. The solutions were sonicated in hot water

bath at 60 ºC for 45 min, followed by further dilution with 4000 µL of 1% HNO_3. All analyses were performed on a PerkinElmer NexION ® 350D ICP-MS using Syngistix™ software (Shelton, CT, USA). To quantify the Au concentration, the calibration curve was developed based on the intensity and concentration of Au under the linear range. Under the optimized instrumental conditions and standard reaction mode, the limit of detection of Au was around 10 ppt, and the limit of quantification of Au was estimated at 50 ppt. The concentration of Au in the cell was determined after obtaining calibration curve of a various gold ion from commercial standards (1, 5, 10, 50 and 100 ng/mL).

Biocompatibility Assay. The cytotoxicity assays of AuNRs before and after PEG passivation were carried out on mouse melanoma cell line B16-F10 using MTT assay. In brief, 5 x 10^3 cells per well were seeded in 96- well plate and incubated for 24 hours. The seeded cells were washed twice with PBS to remove the debris before treatment. Then the medium was replaced with various concentrations of AuNRs (0.01, 0.1, 0.5, 5, 10, 25, and 50 µg/mL) suspended in DMEM. Control cell was maintained without treatment. The excess of particles was removed by washing with PBS. After 24 hours incubation, MTT was added to each well and further incubated for 4h according to the manufacturer recommendation. The dark blue crystals generated by the live cells were dissolved in 100 µL DMSO, and their absorbance was recorded at 570 nm using a microplate reader (BioTek, Synergy H1 hybrid reader).

NIR Mediated Phototoxicity Assay In Vitro. The photothermal effects of Raw AuNR and PEGylated AuNRs on B16-F10 cell line, in the presence and the absence of NIR laser exposure, were conducted using MTT assay. For this purpose, 5 x 10^3 cells per well were seeded in a 96-well plate. When cells nearly reached to 85% confluency, Raw AuNR, AuNR-PEG-2, AuNR-PEG-5, and AuNR-PEG-10 (0.01, 0.1, 0.5, 5, 10, 25, and 50 µg/mL) were added and incubated

for additional 24hr. Cells without AuNR and laser treatment was used as a control. At the end of incubation time, cells were irradiated using a continuous-wave diode laser of wavelength 808 nm with a 1 mm spot focused size at a power of 14.2W/cm^2 for 10 seconds. After laser exposure, cells were incubated for additional 1 h at 37°C humidified with 5% CO_2. The cell viability was conducted by MTT assay.

RESULTS AND DISCUSSION

NIR-responsive AuNRs were synthesized using seed-mediated growth.[15] The formation of AuNR was confirmed by observing its morphology using transmission electron microscopy and reading its longitudinal (LSPR) and transverse surface plasmon resonance (TSPR). The synthesized AuNRs were monodisperse with an aspect ratio of 5.1 ± 0.83 with an average length of 51.2 ± 5.53 nm and width of 10.02 ± 2.17 nm (Figure 1 A). The LSPR and TSPR peaks of the as-synthesized AuNRs were found to be 840 nm and 510 nm, respectively. After surface functionalization with thiolated PEG of different molecular masses, LSPR peaks were found to be 850, 840, and 850 nm for AuNR-PEG-2, AuNR-PEG-5, and AuNR-PEG-10, respectively. Nonetheless, the TSPR peak remained at 510 nm before and after PEGylation (Figure 1B).

Next, the surface coating efficiency of PEG onto the AuNR surfaces was confirmed by measuring hydrodynamic diameter using DLS. The hydrodynamic size of the CTAB stabilized AuNRs was found to be 50.7 ± 0.2 nm in diameter, which when passivated with PEG reached 79.36 ± 0.14, 85.0 ± 1.2, and 80.00 ± 0.13 nm for AuNR-PEG-2, AuNR-PEG-5, and AuNR-PEG-10, respectively (Figure 1C). Additionally, the zeta potentials of Raw AuNR changed from positive +53.7 ± 3.5 mV to negative −21.5 ± 0.4, −24.5 ± 0.5, and −28.3 ± 0.4 mV for AuNR-PEG-2, AuNR-PEG-5, and AuNR-PEG-10. These changes in zeta potential are indicative of successful ligand exchange between CTAB and PEG on the surface of the AuNRs and confirmed

the successful surface functionalization (Figure 1D). The surface functionalized PEG shows higher colloidal stability at 4 °C (Figure S1) over the period.

With PEG modification supported by the DLS and zeta potential results, we moved to characterizing the density of the surface coatings. Thermogravimetric analysis was performed in an inert environment, and the mass of remaining metallic gold was recorded to permit calculation of the mass ratio between PEG and gold in the AuNRs. It is worth noting that metallic gold remains in the sample holder whereas the PEG completely decomposes as CO_2 and other volatile compounds. Therefore, from the residual percentage of metallic gold, the mass fractions of PEG in AuNR-PEG-2, AuNR-PEG-5, and AuNR-PEG-10 were found to be 12%, 12.7% and 18.5%, respectively (Figure 1E). Functionalization of the AuNRs by PEG was further corroborated by FTIR analysis (Figure 1F). The FTIR spectrum of Raw AuNR, AuNR-PEG-2, AuNR-PEG-5, and AuNR-PEG-10 strongly support the replacement of CTAB on the surface of AuNR by the thiol PEGs. The peak at 1100 cm^{-1} is due to the etheral C-O stretching of PEG molecule while the peak at 1600 cm^{-1} is attributed to C–O stretching of the carboxyl group. The broad and very wide peak ranging from 2400 to 3400 cm^{-1} is due to the hydrogen bonded carboxyl group showing the surface replacement of CTAB by PEG moiety.

The photothermal efficiency of the Raw AuNR, AuNR-PEG-2, AuNR-PEG-5, and AuNR-PEG-10 were investigated under 808 nm NIR laser irradiation. All samples suspended in an aqueous solution were irradiated at the continuous wave constant diode laser power of 21.2 W/cm^2 in a cell-free environment where the change in temperature versus time was noted using a thermal imaging system (FLIR Systems). As shown in Figure 2, a time-dependent increase in temperature was observed in all samples. For Raw AuNR, the temperature of the suspension reached up to 56.3 ± 2.9 °C under NIR laser. In the case of AuNR-PEG-2, AuNR-PEG-5, and

AuNR-PEG-10, the change in temperature was 47.1 ± 1.1, 57.1 ± 2.7 and 69.2 ± 2.7 °C, respectively. However, during NIR exposure, a change in the color of the Raw AuNR suspension was observed, which was confirmed by recording the change in LSPR (Figure 3). This is presumably due to the fact that colloidal stability of AuNR is greatly affected by the local temperature, and high local temperature makes Raw AuNRs unstable in the suspension (Scheme 1). To further elucidate the effect of NIR laser exposure on different PEG-modified AuNRs, we conducted a photothermal experiment where we measured the temperature at the top (point of NIR laser contact), middle, and bottom of the AuNR suspension. The distance between the top, middle and bottom positions were approximately 10 mm in depth. Figure 2 demonstrates that the temperature distribution was highly nonuniform in the case of AuNR-PEG-10, with a substantial change in temperature from 69.2 ± 2.7 °C at the top (at the point of laser contact) to 18.2 ± 0.8 °C at the bottom. The other AuNRs show more uniformity in temperature. These results suggest that higher molecular mass PEG may thermally insulate the AuNRs, supporting a higher temperature gradient.

Changes in the structural integrity and plasmonic properties of the AuNRs after NIR irradiation were investigated transmission electron microscopy and UV-Vis spectrometry. As shown in Figure 3A, the Raw AuNRs and AuNR-PEG-2 show drastic changes in their LSPR peaks after NIR irradiation, which is possibly due to the temperature induced erosion of the AuNRs. For AuNR-PEG-5 and AuNR-PEG-10, the LSPR signals were quite stable even after NIR irradiation, which confirms the thermal stability of AuNRs after PEG grafting without negatively affecting their photothermal properties.

To better understand how the PEG coatings affected the heat conduction from the AuNR surfaces, we performed molecular dynamics simulations of PEG-conjugated gold surfaces and

calculated the thermal conductivity through the PEG brushes. To make the simulations feasible and simplify the analysis, we did not model complete AuNRs, but simply considered the structure of the PEG brush on flat slabs of gold. First, we compared the conductivity of a bare gold slab (Table 1, System A) to two models coated with PEG-SH molecules of different masses, mimicking the experiments. Systems B and C were conjugated with 2 and 5 kDa PEG molecules at densities of 1.98 and 0.86 molecules/nm^2 , respectively, representing two types of nanorods used in the experiments (AuNR-PEG-2 and AuNR-PEG-5) (Figure 4). After relaxation, the 2 kDa PEG brushes appeared as shown in Figure 4A. In this case, the 2 kDa PEG chains completely crowd the surface, leaving little access to water. Indeed, the graph of the water density, Figure 4B, shows essentially no water within 4 nm of the gold surface, while the density of PEG near the gold surface is roughly the value of solid PEG. On the other hand, at the lower density of 5 kDa PEG molecules in System C, we observed less crowding of PEG near the surface, with significant amounts of water penetrating the brush. Because of the greater length of the PEG molecules, the brush in System C extended farther from the gold surface than of System B, reaching beyond 8 nm from the surface.

The thermal conductivity of the two PEG-containing systems and the bare gold system were calculated as described previously[46] and detailed in the Methods section, by applying a constant heat current between a segment of the system near $z = 0$ and a segment of the system near $z = \pm 8.9$ nm. Due to the use of periodic boundary conditions, the positions $z = \pm 8.9$ nm are equivalent and in physical contact. The exact heat current depended slightly on the number of water molecules in each segment of the system, but in all cases the average was in the range of 2.1–2.4 μW. The average temperature distributions for the bare and PEG-coated slabs after reaching the steady-state are shown in Figure 4C. In the case of the bare slab, the calculation was

simply a measurement of the thermal conductivity of bulk model water—being a uniform medium, the temperature distribution appears linear. The thermal conductivity, as determined by the slope of this distribution is 1.03±0.02 W/(m·K), shown in Table 1, is about 60% larger than that for real water at the same temperature[47] which is not surprising due to the fact that the flexible TIP3P water model used in the simulations has a higher self-diffusion coefficient than real water.[48] The temperature distribution of the PEG-coated gold surfaces (Figure 4C) is not uniform, due to the heterogeneity of these systems. The slope of the temperature profile is greatest for $1.4<|z|<4.8$ nm, which also corresponds to the region of greatest PEG density (Figure 4B). The net temperature changes through the PEG brushes and water layer were 84 and 89 °C , more than twice that in the pure water system (39 °C), leading to proportionately smaller conductivities. Although the temperature fell below 0 °C (Figure 4B) in some places, freezing was not and cannot be observed in these simulations.[49] The simulations support the notion that PEG conjugation acts to thermally insulate the gold nanorods from their environment, in agreement with the larger temperature gradients observed for the PEGylated nanorods in the experiment. Furthermore, as indicated in Table 1, the thermal conductivity was smaller for the long 5 kDa PEG brush (System C) than for the shorter, higher density brush (System B), in agreement with the trend measured in the experiments.

The cellular internalization efficiencies of Raw and PEG-modified AuNRs were investigated in mouse melanoma cell line B16-F10 using hyperspectral dark-field microscopy and ICP-MS. ICP-MS was used to evaluate the amount of gold taken up by cells after 6 and 24 hours of exposure. After 6 h of incubation, the cellular uptake efficiencies of Raw AuNR, AuNR-PEG-2, AuNR-PEG-5, and AuNR-PEG-10 were found to be 44, 23, 32 and 30%, respectively (Figure 5 A). For 24 h of incubation, the cellular uptake efficiency of Raw AuNR, AuNR-PEG-2, AuNR-

PEG-5, and AuNR-PEG-10 were found to be 48, 28, 30 and 32%, respectively. The results indicate that the number of AuNRs taken up by B16-F10 cell is significantly greater for Raw AuNRs than for PEG-functionalized AuNRs. It is evident that PEGylation reduces the endocytosis of NPs and thus reduces its cellular internalization. No significant change was observed between different PEG-modified AuNRs even after 6 and 24 h incubation. It has previously been suggested that AuNRs are taken up via endocytosis and localized in endosomes within the cell.[50] Further qualitative analysis with hyperspectral dark-field imaging shows that Raw and PEG-modified AuNRs were taken up by the cells without significant loss of their structural integrity, as evidenced by their plasmonic signals inside the cell (Figure 5B, lower panel). The *in vitro* viability of cells containing Raw and PEG-coated AuNRs in the presence and the absence of the NIR laser was investigated in mouse melanoma B16-F10 cell lines after 24 h of AuNR treatment. For the photothermal therapy experiments, after 24 hours of treatment, the cell was irradiated with an NIR laser of wavelength 808 nm (14.1 W/cm^2) for 10 seconds. Cell viability as a function of AuNR dose was observed (Figure 6).

For the Raw AuNRs, low cell viability was observed, even at a low dose of 0.5 μg/mL, likely due to the cytotoxicity of residual CTAB surfactant. At the highest concentration tested (25 μg/mL), the viability of cells with Raw AuNRs was found to be 20% in the presence of NIR radiation and 24% in its absence, a difference that was not statistically significant. In comparison with Raw AuNRs, PEG-functionalized AuNRs (in the absence of NIR radiation) were found to be biocompatible with B16-F10 cells. At the highest concentration (25 μg/mL) tested, the viability of AuNR-PEG-2 treated cells was found to 60% in the absence of NIR radiation, but was reduced to 28% after 10 s of NIR radiation. For AuNR-PEG-5, the cell viability was found to be 38% and 60% in the presence and absence of NIR radiation, respectively. For AuNR-PEG-

10, the cell viability was found to be 30% and 60% in the presence and absence of NIR radiation. Therefore, for the PEG-modified AuNRs, we observed a significant reduction in cell viability caused by irradiation from the NIR laser, in contrast the the Raw AuNRs. Most importantly, among different the different PEG modifications, AuNR-PEG-5 exhibited significant phototoxicity even at the lowest concentration tested (0.5 μg/mL), while higher concentrations were required to observe significant NIR-radiation-induced toxicity for AuNR-PEG- 2 and AuNR-PEG-10. The superior performance of AuNR-PEG-5 over the other AuNRs can be explained by Figure 3. During NIR treatment, the AuNR-PEG-2 nanorods appear to have been partially destroyed, as evident from the change in their dramatic change in aspect ratio shown in Figure 3B **[~~FIGURE 3B DOES NOT HAVE AuNR-PEG-2 in the absence of NIR radiation~~]**, resulting in a relatively small maximum temperature change of 10±1 °C in the cell suspension (Figure 7B). Similarly, for AuNR-PEG-10, the thickness of the PEG brush hinders the NIR and AuNR surface contact. Figure 7D, provides great evidence of the pronounced effect in the case of AuNR-PEG-5, where the cell suspension temperature reaches to 20 ± 1.2 °C, thereby confirming our hypothesis and results obtained from both experiment and molecular simulation.

CONCLUSIONS

In this study, we determined the influence of the PEG coating of the AuNRs on their production of hyperthermia, with the aim improving photothermal therapy of cancer. We compared unmodified, CTAB-stabilized AuNRs (Raw) with three PEG coatings of different PEG molecular masses (2, 5, and 10 kDa). AuNR-PEG-2 has a denser PEG coating than that of AuNR-PEG-5 and AuNR-PEG-10 as demonstrated by molecular simulation and supported by the quantitative thermogravimetric analysis. **Therefore, there is little room for AuNR-PEG-2 on its surface for water diffusion as compared to the AuNR-PEG-10. However, due to**

intermediate chain length and relatively less dense coating of 5 kDa induce more heat. Under an NIR laser, AuNR-PEG-5 shows a higher degree of structural stability and more uniform temperature distribution with enhanced NIR induced thermal toxicity against mouse melanoma cell line, B16-F10. Therefore, this comprehensive fundamental study suggested an optimum polymer length of 5 kDa of PEG is advantageous for better surface passivation and colloidal stability of AuNR, which also maximizes the heat conduction from the nanorod–fluid interface to the surroundings to enhance its photothermal efficiency. Overall, this study illustrates the need for a proper selection of surface functionalizing agent in rationale design of AuNRs for biomedical applications.

Acknowledgments

The authors acknowledge the support from the Johnson Cancer Research Center, Department of Chemistry, and the Nanotechnology Innovation Center of Kansas State (NICKS), Kansas State University, Manhattan, Kansas. This work was also supported in part by a grant from the National Science Foundation (CHE-1726332).

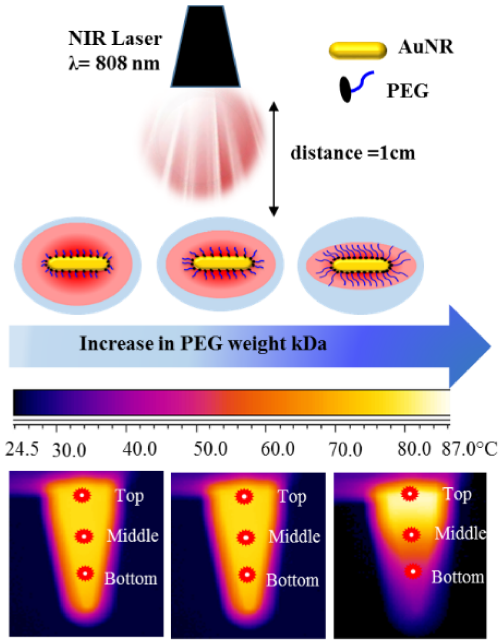

Scheme 1. Schematic showing the effect of surface passivation of gold nanorods with PEG molecules of various molecular masses (2, 5, and 10 kDa) on plasmonic heating.

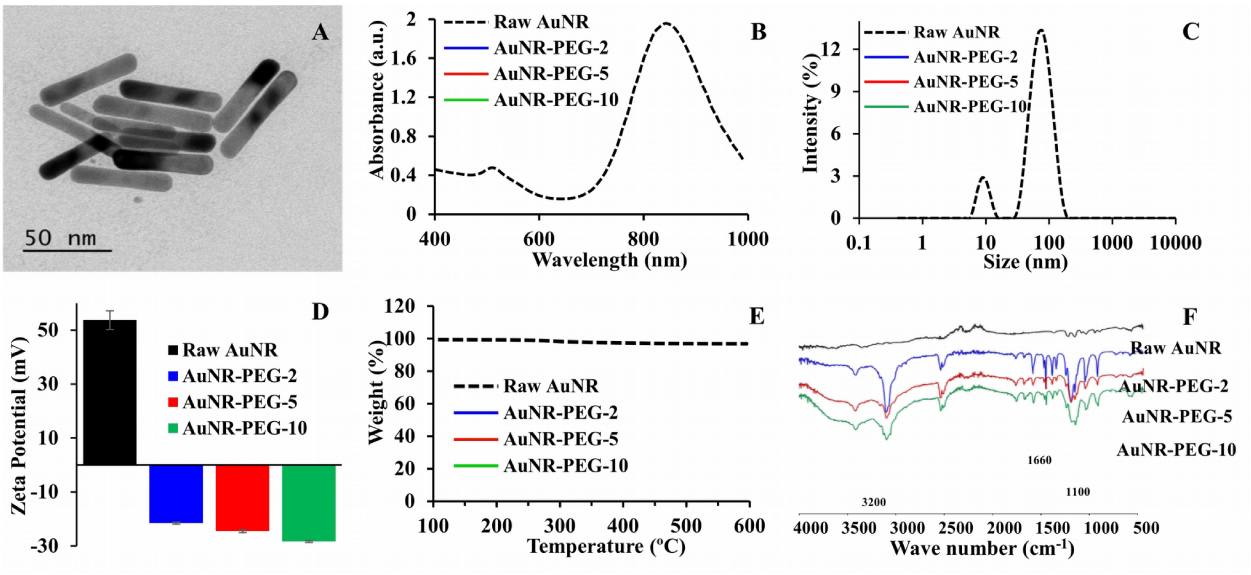

Figure 1. Physiochemical characterization of AuNRs before and after surface functionalization. (A) A representative transmission electron micrograph of as-synthesized AuNRs. (B) Surface plasmon resonance spectrum of NIR-responsive AuNRs before and after surface functionalization using PEG molecules of different molecular weights (viz., 2, 5, 10 kDa). (C) and (D) are the hydrodynamic size and zeta potential before and after PEG functionalization. (E) Thermogravimetric analysis for quantitative determination of PEG functionalization. (F) FTIR spectrum of the AuNRs, verifying PEG conjugation on the surface of the AuNRs. The number 2, 5, and 10 in the nomenclature of each sample represents the corresponding molecular mass of the PEG molecules in kDa.

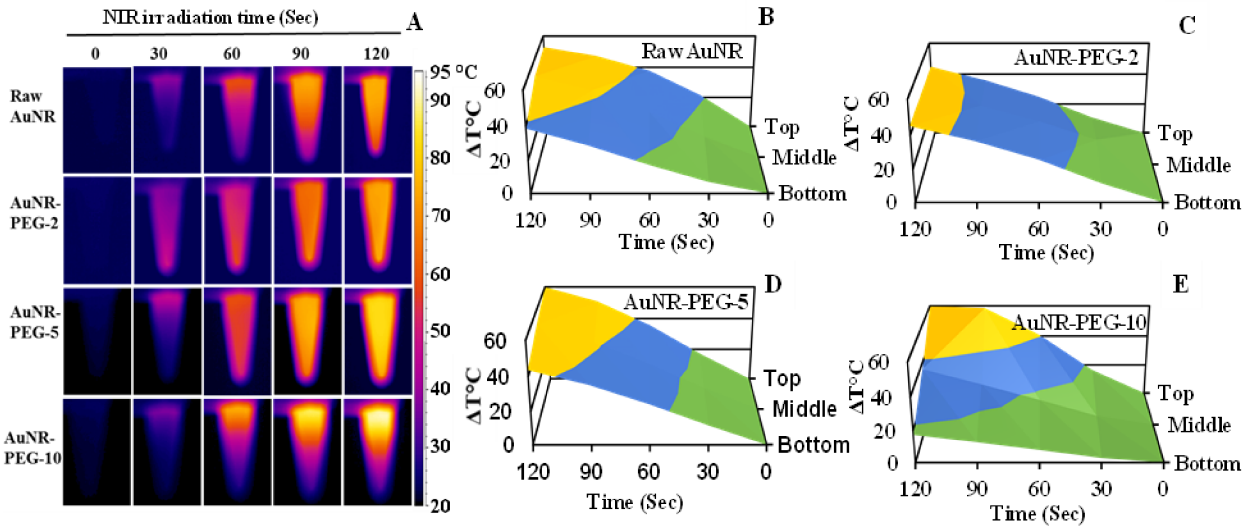

Figure 2. Photothermal properties of Raw and PEG-functionalized AuNRs. (A) Various AuNR aqueous suspensions were irradiated with a near-infrared laser (λ=808 nm, 21.2 W/cm^2) for 120 seconds and the evolution of temperature throughout the suspension was recorded using FLIR thermal camera system. (B), (C), (D), and (E) are the 3D temperature plots showing the average change in temperature as a function of time measured at the top, middle, and bottom of the AuNR suspension of Raw AuNRs, AuNR-PEG-2, AuNR-PEG-5, and AuNR-PEG-10, respectively.

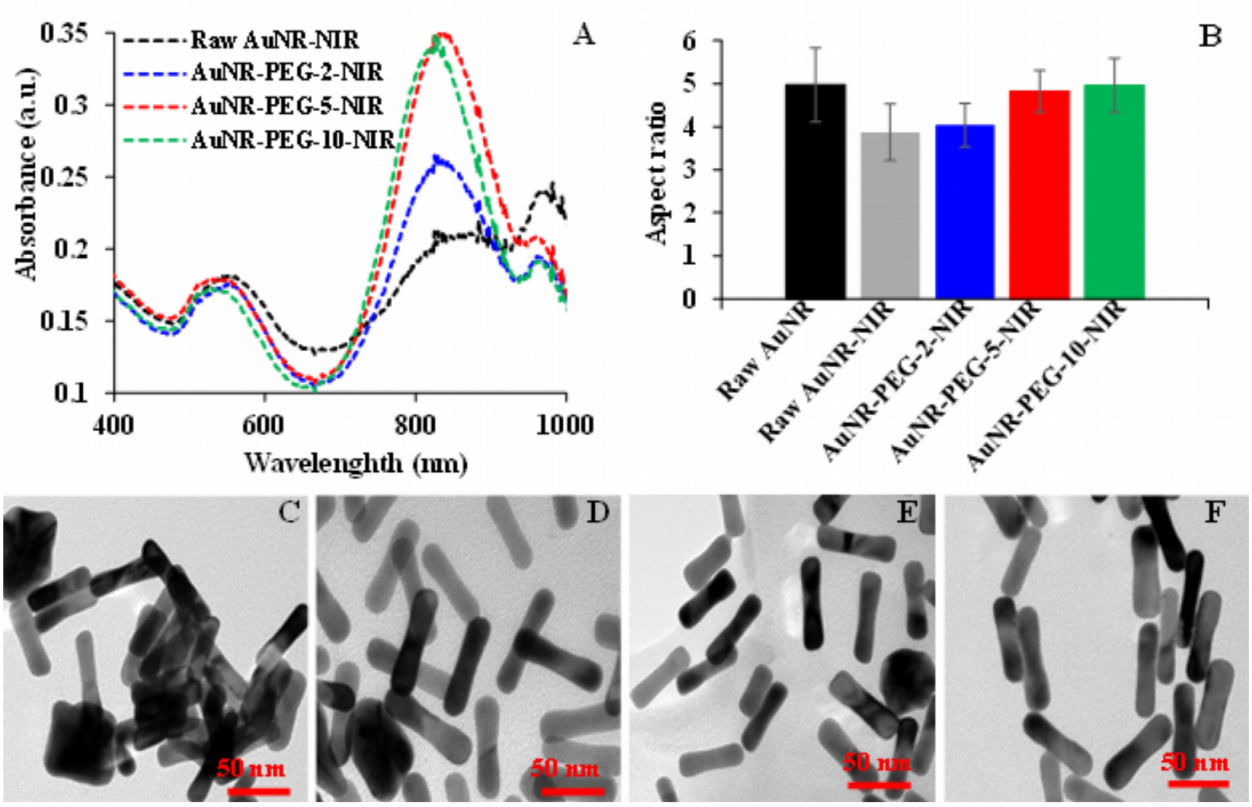

Figure 3. LSPR response and alteration in AuNR aspect ratio after NIR exposure of Raw and PEG passivated AuNRs. (A) UV-Vis spectrum showing changes in LSPR after NIR heating of both Raw and PEG passivated AuNRs. (B) The average aspect ratio of both Raw and PEG-functionalized AuNR before and after NIR heating. (C) Raw AuNR-NIR, (D) AuNR-PEG-2-NIR, (E) AuNR-PEG-5-NIR, and (F) AuNR-PEG-10-NIR are the representative transmission electron micrographs. Aspect ratio was calculated by measuring the length and width of 100 nanorods per sample. Scale bar 50nm.

Table 1. Thermal conductivity calculated in molecular dynamics simulations for PEG brushes of different PEG molecular masses and chain densities on a gold surface. The simulation systems were constructed for direct comparison to the experiments.

Simulation system	**PEG molecular mass [kDa]**	**PEG chain density [nm^{-2}]**	**Thermal cond. [W/(K·m)]**
A	–	0.0	1.03 ± 0.02
B	2.0	1.98	0.45 ± 0.01
C	5.0	0.86	0.40 ± 0.01

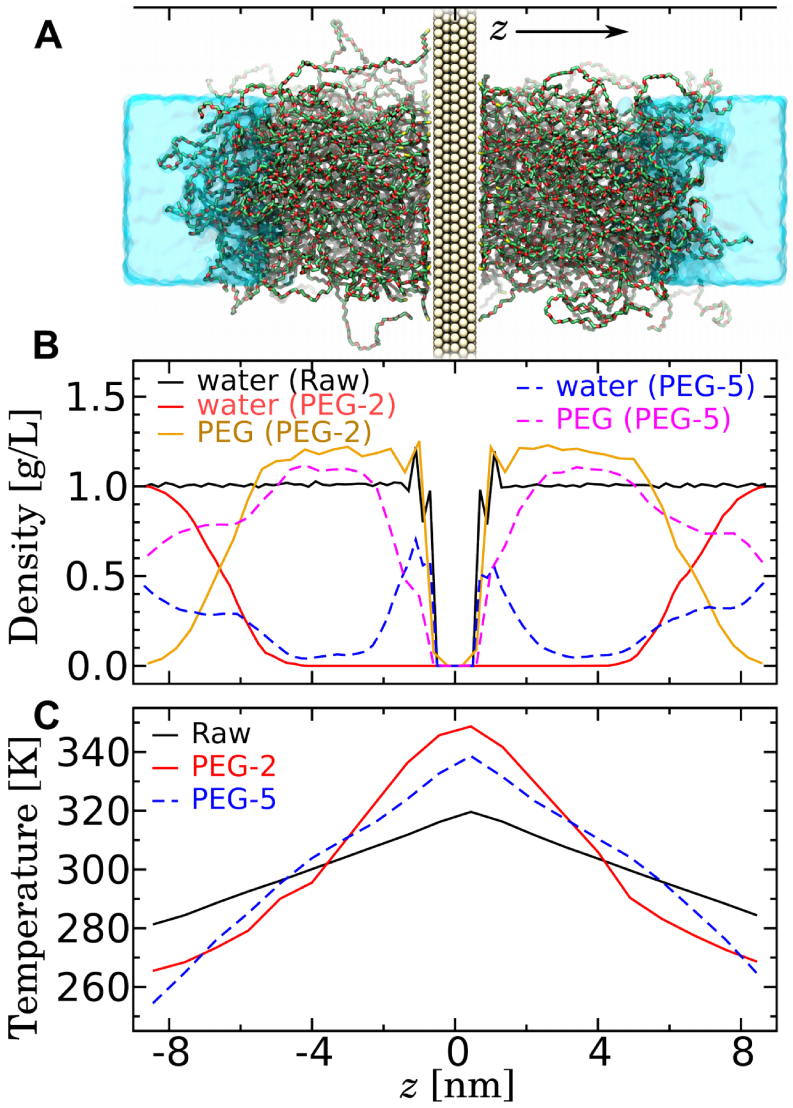

Figure 4. Molecular dynamics simulations of heat conduction through PEG brushes. (A) Snapshot of simulation System B for gold conjugated with 2 kDa PEG. The gold slab is shown as pale yellow spheres. The thiolated PEG molecules, illustrated in a bonds representation, are colored by atom type (C, green; O, red; S, yellow). For clarity, H atoms are not shown and the explicit water molecules are illustrated as a cyan surface. Due to the use of periodic boundary conditions, the left and right ends of the system are in physical contact, and the PEG-coated gold surfaces have effectively infinite extent in the *xy* plane. (B) Mass density of water and PEG as a function of the *z* coordinate for Systems A (Raw), B (2 kDa PEG), and C (5 kDA PEG). The *z* scale is faithfully aligned with the image in panel A. (C) Steady-state temperature distribution in simulations where a constant heat current was induced in the system, permitting the thermal

conductivity to be calculated. The larger temperature differences observed for the PEG-containing systems imply smaller thermal conductivities.

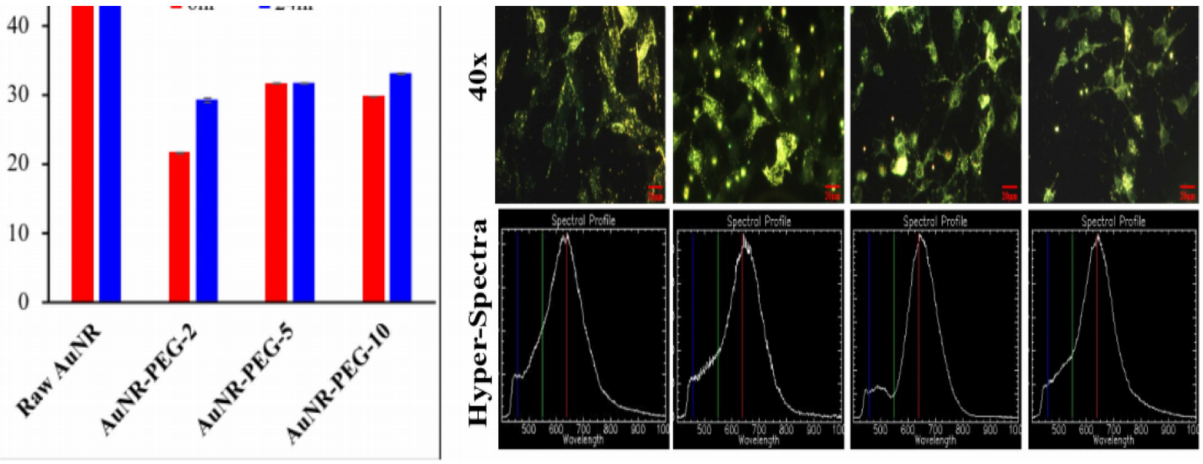

Figure 5. Cellular uptake efficiency of Raw and PEG-functionalized AuNRs with mouse melanoma cell line (B16-F10). (A) Quantitative cellular uptake of AuNRs at incubation times of 6 and 24 h as measured by ICP-MS, and (B) Dark field hyperspectral microscopic images of B16-F10 cells treated with Raw and PEGylated AuNRs, and corresponding hyperspectral graph (lower panel) indicating the structural integrity of AuNRs inside the cells. Both LSPR and TSPR are visible, which is characteristic of AuNRs.

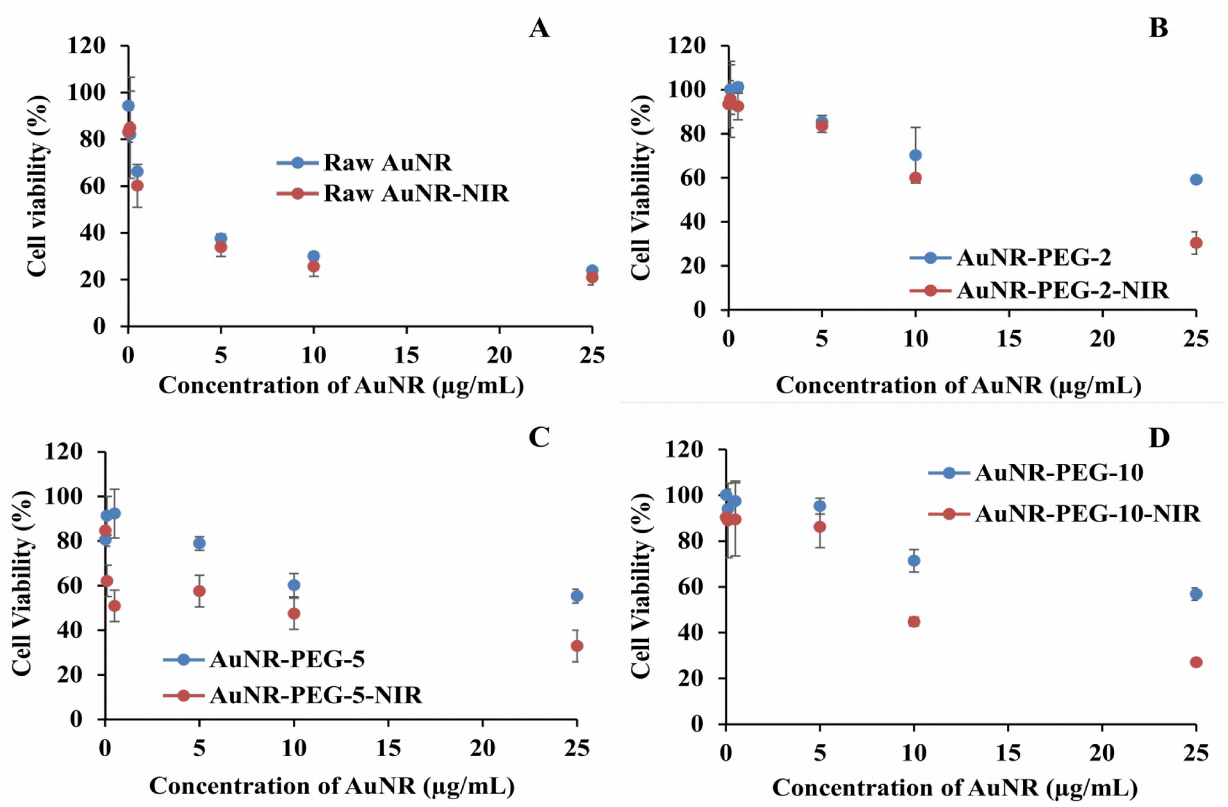

Figure 6. In vitro phototoxicity of Raw and PEG-functionalized AuNRs against B16-F10 Cells. (A) Raw AuNRs, (B) AuNR-PEG-2, (C) AuNR-PEG-5, and (D) AuNR-PEG-10 before and after laser irradiation (irradiation time=10 s; λ=808 nm; power= 14.1 W/cm^2).

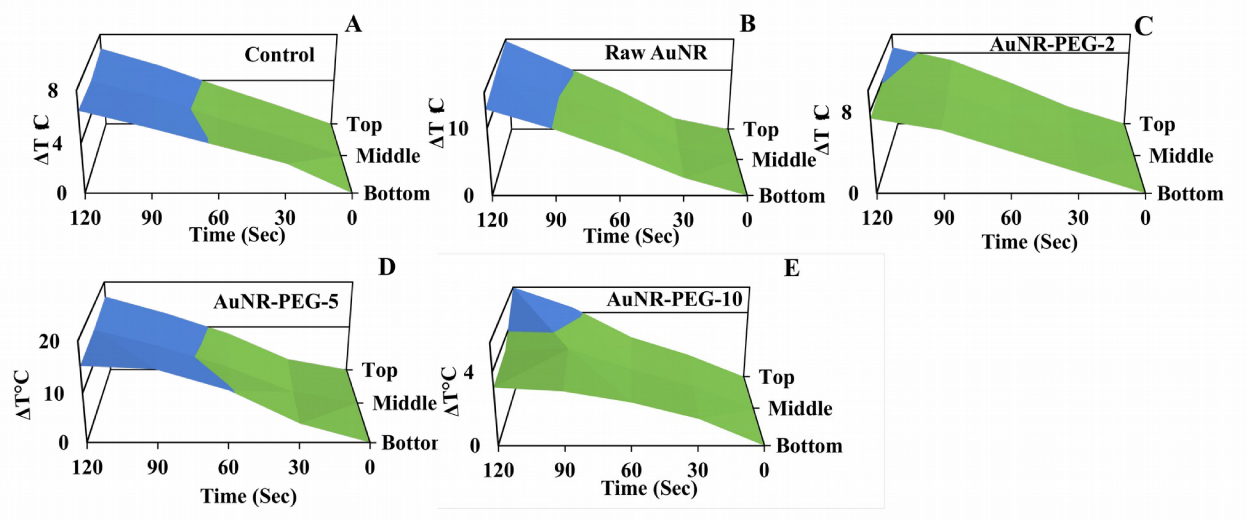

Figure 7. Photothermal properties of Raw and PEG-functionalized AuNRs under laser irradiation (λ=808 nm, 21.2 W/cm^2) in the cell suspension. The cells were previously incubated with AuNRs for 24 h and recovered as a cell suspension to study the NIR-mediated thermal effect. A, B, C, D, and E are the 3D temperature plots showing the average change in temperature at the top, middle, and bottom of the cell suspension. Cells without AuNRs was used as a control. Note that the vertical (ΔT) axis differs among the plots. (A), Raw AuNR (B), AuNR-PEG-2 (C), AuNR-PEG-5 (D), and AuNR-PEG-10 (E).

References.

(1) Stone, J.; Jackson, S.; Wright, D. Biological Applications of Gold Nanorods. *Wiley Interdiscip. Rev. Nanomed. Nanobiotechnol.* **2011**, *3* (1), 100–109.

(2) Yang, D.-P.; Cui, D.-X. Advances and Prospects of Gold Nanorods. *Chem. – Asian J.* **2008**, *3* (12), 2010–2022.

(3) Huang, H.; He, C.; Zeng, Y.; Xia, X.; Yu, X.; Yi, P.; Chen, Z. Preparation and Optical Properties of Worm-like Gold Nanorods. *J. Colloid Interface Sci.* **2008**, *322* (1), 136–142.

(4) Gui, C.; Cui, D. Functionalized Gold Nanorods for Tumor Imaging and Targeted Therapy. *Cancer Biol. Med.* **2012**, *9* (4), 221.

(5) Boisselier, E.; Astruc, D. Gold Nanoparticles in Nanomedicine: Preparations, Imaging, Diagnostics, Therapies and Toxicity. *Chem. Soc. Rev.* **2009**, *38* (6), 1759–1782.

(6) Murphy, C. J.; Gole, A. M.; Stone, J. W.; Sisco, P. N.; Alkilany, A. M.; Goldsmith, E. C.; Baxter, S. C. Gold Nanoparticles in Biology: Beyond Toxicity to Cellular Imaging. *Acc. Chem. Res.* **2008**, *41* (12), 1721–1730.

(7) Aryal, S.; Nguyen, T. D. T.; Pitchaimani, A.; Shrestha, T. B.; Biller, D.; Troyer, D. Membrane Fusion-Mediated Gold Nanoplating of Red Blood Cell: A Bioengineered CT-Contrast Agent. *ACS Biomater. Sci. Eng.* **2017**, *3* (1), 36–41.

(8) Huang, X.; Jain, P. K.; El-Sayed, I. H.; El-Sayed, M. A. Plasmonic Photothermal Therapy (PPTT) Using Gold Nanoparticles. *Lasers Med. Sci.* **2008**, *23* (3), 217–228.

(9) Gormley, A. J.; Larson, N.; Banisadr, A.; Robinson, R.; Frazier, N.; Ray, A.; Ghandehari, H. Plasmonic Photothermal Therapy Increases the Tumor Mass Penetration of HPMA Copolymers. *J. Control. Release Off. J. Control. Release Soc.* **2013**, *166* (2), 130–138.

(10) Weissleder, R. A clearer vision for *in vivo* imaging https://www.nature.com/articles/nbt0401_316 (accessed Nov 27, 2017).

(11) Smith, A. M.; Mancini, M. C.; Nie, S. Second Window for in Vivo Imaging. *Nat. Nanotechnol.* **2009**, *4* (11), 710–711.

(12) Chen, H.; Guan, Y.; Wang, S.; Ji, Y.; Gong, M.; Wang, L. Turn-on Detection of a Cancer Marker Based on near-Infrared Luminescence Energy Transfer from NaYF4:Yb,Tm/NaGdF4 Core-Shell Upconverting Nanoparticles to Gold Nanorods. *Langmuir ACS J. Surf. Colloids* **2014**, *30* (43), 13085–13091.

(13) Liu, Y.; Yang, M.; Zhang, J.; Zhi, X.; Li, C.; Zhang, C.; Pan, F.; Wang, K.; Yang, Y.; Martinez de la Fuentea, J.; et al. Human Induced Pluripotent Stem Cells for Tumor Targeted Delivery of Gold Nanorods and Enhanced Photothermal Therapy. *ACS Nano* **2016**, *10* (2), 2375–2385.

(14) Aryal, S.; KC, R. B.; Dharmaraj, N.; Bhattarai, N.; Kim, C. H.; Kim, H. Y. Spectroscopic Identification of SAu Interaction in Cysteine Capped Gold Nanoparticles. *Spectrochim. Acta. A. Mol. Biomol. Spectrosc.* **2006**, *63* (1), 160–163.

(15) Arunkumar, P.; Raju, B.; Vasantharaja, R.; Vijayaraghavan, S.; Preetham Kumar, B.; Jeganathan, K.; Premkumar, K. Near Infra-Red Laser Mediated Photothermal and Antitumor Efficacy of Doxorubicin Conjugated Gold Nanorods with Reduced Cardiotoxicity in Swiss Albino Mice. *Nanomedicine Nanotechnol. Biol. Med.* **2015**, *11* (6), 1435–1444.

(16) de Dios, A. S.; Díaz-García, M. E. Multifunctional Nanoparticles: Analytical Prospects. *Anal. Chim. Acta* **2010**, *666* (1–2), 1–22.

(17) Aryal, S.; Grailer, J. J.; Pilla, S.; Steeber, D. A.; Gong, S. Doxorubicin Conjugated Gold Nanoparticles as Water-Soluble and P^{H}-Responsive Anticancer Drug Nanocarriers. *J. Mater. Chem.* **2009**, *19* (42), 7879–7884.
(18) Huang, X.; Jain, P. K.; El-Sayed, I. H.; El-Sayed, M. A. Gold Nanoparticles: Interesting Optical Properties and Recent Applications in Cancer Diagnostics and Therapy. *Nanomed.* **2007**, *2* (5), 681–693.
(19) Kennedy, L. C.; Bickford, L. R.; Lewinski, N. A.; Coughlin, A. J.; Hu, Y.; Day, E. S.; West, J. L.; Drezek, R. A. A New Era for Cancer Treatment: Gold-Nanoparticle-Mediated Thermal Therapies. *Small Weinh. Bergstr. Ger.* **2011**, *7* (2), 169–183.
(20) Nolsøe, C. P.; Torp-Pedersen, S.; Burcharth, F.; Horn, T.; Pedersen, S.; Christensen, N. E.; Olldag, E. S.; Andersen, P. H.; Karstrup, S.; Lorentzen, T. Interstitial Hyperthermia of Colorectal Liver Metastases with a US-Guided Nd-YAG Laser with a Diffuser Tip: A Pilot Clinical Study. *Radiology* **1993**, *187* (2), 333–337.
(21) Vogl, T.; Mack, M.; Straub, R.; Zangos, S.; Woitaschek, D.; Eichler, K.; Engelmann, K. [Thermal ablation of liver metastases. Current status and prospects]. *Radiol.* **2001**, *41* (1), 49–55.
(22) Tong, L.; Zhao, Y.; Huff, T. B.; Hansen, M. N.; Wei, A.; Cheng, J.-X. Gold Nanorods Mediate Tumor Cell Death by Compromising Membrane Integrity. *Adv. Mater.* **2007**, *19* (20), 3136–3141.
(23) Hirsch, L. R.; Stafford, R. J.; Bankson, J. A.; Sershen, S. R.; Rivera, B.; Price, R. E.; Hazle, J. D.; Halas, N. J.; West, J. L. Nanoshell-Mediated near-Infrared Thermal Therapy of Tumors under Magnetic Resonance Guidance. *Proc. Natl. Acad. Sci.* **2003**, *100* (23), 13549–13554.
(24) O'Neal, D. P.; Hirsch, L. R.; Halas, N. J.; Payne, J. D.; West, J. L. Photo-Thermal Tumor Ablation in Mice Using near Infrared-Absorbing Nanoparticles. *Cancer Lett.* **2004**, *209* (2), 171–176.
(25) Link, S.; El-Sayed, M. A. Shape and Size Dependence of Radiative, Non-Radiative and Photothermal Properties of Gold Nanocrystals. *Int. Rev. Phys. Chem.* **2000**, *19* (3), 409–453.
(26) Kelly, K. L.; Coronado, E.; Zhao, L. L.; Schatz, G. C. The Optical Properties of Metal Nanoparticles: The Influence of Size, Shape, and Dielectric Environment. *J. Phys. Chem. B* **2003**, *107* (3), 668–677.
(27) Liu, X.; Huang, N.; Li, H.; Wang, H.; Jin, Q.; Ji, J. Multidentate Polyethylene Glycol Modified Gold Nanorods for in Vivo Near-Infrared Photothermal Cancer Therapy. *ACS Appl. Mater. Interfaces* **2014**, *6* (8), 5657–5668.
(28) Gobeli, D. A.; Yang, J. J.; El-Sayed, M. A. Laser Multiphoton Ionization-Dissociation Mass Spectrometry. *Chem. Rev.* **1985**, *85* (6), 529–554.
(29) Dickerson, E. B.; Dreaden, E. C.; Huang, X.; El-Sayed, I. H.; Chu, H.; Pushpanketh, S.; McDonald, J. F.; El-Sayed, M. A. Gold Nanorod Assisted Near-Infrared Plasmonic Photothermal Therapy (PPTT) of Squamous Cell Carcinoma in Mice. *Cancer Lett.* **2008**, *269* (1), 57–66.
(30) Harris, J. M.; Chess, R. B. Effect of Pegylation on Pharmaceuticals. *Nat. Rev. Drug Discov.* **2003**, *2* (3), 214.
(31) Huff, T. B.; Hansen, M. N.; Zhao, Y.; Cheng, J.-X.; Wei, A. Controlling the Cellular Uptake of Gold Nanorods. *Langmuir* **2007**, *23* (4), 1596–1599.

(32) Liao, H.; Hafner, J. H. Gold Nanorod Bioconjugates. *Chem. Mater.* **2005**, *17* (18), 4636–4641.
(33) Niidome, T.; Yamagata, M.; Okamoto, Y.; Akiyama, Y.; Takahashi, H.; Kawano, T.; Katayama, Y.; Niidome, Y. PEG-Modified Gold Nanorods with a Stealth Character for in Vivo Applications. *J. Control. Release Off. J. Control. Release Soc.* **2006**, *114* (3), 343–347.
(34) Chen, X.; Hou, Y.; Tohme, M.; Park, R.; Khankaldyyan, V.; Gonzales-Gomez, I.; Bading, J. R.; Laug, W. E.; Conti, P. S. Pegylated Arg-Gly-Asp Peptide: 64Cu Labeling and PET Imaging of Brain Tumor Avβ3-Integrin Expression. *J. Nucl. Med.* **2004**, *45* (10), 1776–1783.
(35) von Maltzahn, G.; Park, J.-H.; Agrawal, A.; Bandaru, N. K.; Das, S. K.; Sailor, M. J.; Bhatia, S. N. Computationally Guided Photothermal Tumor Therapy Using Long-Circulating Gold Nanorod Antennas. *Cancer Res.* **2009**, *69* (9), 3892–3900.
(36) Pitchaimani, A.; Nguyen, T. D. T.; Wang, H.; H. Bossmann, S.; Aryal, S. Design and Characterization of Gadolinium Infused Theranostic Liposomes. *RSC Adv.* **2016**, *6* (43), 36898–36905.
(37) Pitchaimani, A.; Nguyen, T. D. T.; Koirala, M.; Zhang, Y.; Aryal, S. Impact of Cell Adhesion and Migration on Nanoparticle Uptake and Cellular Toxicity. *Toxicol. In Vitro* **2017**, *43* (Supplement C), 29–39.
(38) Aryal, S.; Hu, C.-M. J.; Zhang, L. Polymer−Cisplatin Conjugate Nanoparticles for Acid-Responsive Drug Delivery. *ACS Nano* **2010**, *4* (1), 251–258.
(39) Huff, T. B.; Tong, L.; Zhao, Y.; Hansen, M. N.; Cheng, J.-X.; Wei, A. Hyperthermic Effects of Gold Nanorods on Tumor Cells. *Nanomed.* **2007**, *2* (1), 125–132.
(40) Koirala, M. B.; Nguyen, T. D. T.; Pitchaimani, A.; Choi, S.-O.; Aryal, S. Synthesis and Characterization of Biomimetic Hydroxyapatite Nanoconstruct Using Chemical Gradient across Lipid Bilayer. *ACS Appl. Mater. Interfaces* **2015**, *7* (49), 27382–27390.
(41) Ge, Z.; Cahill, D. G.; Braun, P. V. AuPd Metal Nanoparticles as Probes of Nanoscale Thermal Transport in Aqueous Solution. *J. Phys. Chem. B* **2004**, *108* (49), 18870–18875.
(42) Schmidt, A. J.; Alper, J. D.; Chiesa, M.; Chen, G.; Das, S. K.; Hamad-Schifferli, K. Probing the Gold Nanorod−Ligand−Solvent Interface by Plasmonic Absorption and Thermal Decay. *J. Phys. Chem. C* **2008**, *112* (35), 13320–13323.
(43) Huang, J.; Park, J.; Wang, W.; Murphy, C. J.; Cahill, D. G. Ultrafast Thermal Analysis of Surface Functionalized Gold Nanorods in Aqueous Solution. *ACS Nano* **2013**, *7* (1), 589–597.
(44) Pitchaimani, A.; Nguyen, T. D. T.; Maurmann, L.; Key, J.; Bossmann, S. H.; Aryal, S. Gd3 + Tethered Gold Nanorods for Combined Magnetic Resonance Imaging and Photo-Thermal Therapy. *J. Biomed. Nanotechnol.* **2017**, *13* (4), 417–426.
(45) Plimpton, S. Fast Parallel Algorithms for Short-Range Molecular Dynamics. *J. Comput. Phys.* **1995**, *117* (1), 1–19.
(46) Müller-Plathe, F. A Simple Nonequilibrium Molecular Dynamics Method for Calculating the Thermal Conductivity. *J. Chem. Phys.* **1997**, *106* (14), 6082–6085.
(47) Kell, G. S. Thermodynamic and Transport Properties of Fluid Water. In *The Physics and Physical Chemistry of Water*; Water; Springer, Boston, MA, 1972; pp 363–412.
(48) Mark, P.; Nilsson, L. Structure and Dynamics of the TIP3P, SPC, and SPC/E Water Models at 298 K. *J. Phys. Chem. A* **2001**, *105* (43), 9954–9960.

(49) Vega, C.; Sanz, E.; Abascal, J. L. F. The Melting Temperature of the Most Common Models of Water. *J. Chem. Phys.* **2005**, *122* (11), 114507.
(50) Grabinski, C.; Schaeublin, N.; Wijaya, A.; D'Couto, H.; Baxamusa, S. H.; Hamad-Schifferli, K.; Hussain, S. M. Effect of Gold Nanorod Surface Chemistry on Cellular Response. *ACS Nano* **2011**, *5* (4), 2870–2879.